Spin Hall effect investigated by spin Hall magnetoresistance in $Pt_{100-x}Au_x$/CoFeB systems

Cite as: AIP Advances **9**, 125312 (2019); https://doi.org/10.1063/1.5129889
Submitted: 02 October 2019 . Accepted: 04 November 2019 . Published Online: 19 December 2019

Yoshiaki Saito, Nobuki Tezuka, Shoji Ikeda, Hideo Sato, and Tetsuo Endoh

Spin Hall effect investigated by spin Hall magnetoresistance in $Pt_{100-x}Au_x$/CoFeB systems

Cite as: AIP Advances 9, 125312 (2019); doi: 10.1063/1.5129889
Presented: 7 November 2019 • Submitted: 2 October 2019 •
Accepted: 4 November 2019 • Published Online: 19 December 2019

Yoshiaki Saito,[1,a)] Nobuki Tezuka,[2,3] Shoji Ikeda,[1,3,4] Hideo Sato,[1,3,4,5] and Tetsuo Endoh[1,3,4,5,6]

AFFILIATIONS

[1]Center for Innovative Integrated Electronic Systems, Tohoku University, Sendai 980-0845, Japan
[2]Department of Materials Science, Graduate School of Engineering, Tohoku University, Sendai 980-8579, Japan
[3]Center for Spintronics Research Network, Tohoku University, Sendai 980-8577, Japan
[4]Center for Science and Innovation in Spintronics (Core Research Cluster), Tohoku University, Sendai 980-8577, Japan
[5]Research Institute of Electrical Communication, Tohoku University, Sendai 980-8577, Japan
[6]Department of Electrical Engineering, Graduate School of Engineering, Tohoku University, Sendai 980-8579, Japan

Note: This paper was presented at the 64th Annual Conference on Magnetism and Magnetic Materials.
[a)]**E-mail address:** ysaito@cies.tohoku.ac.jp

ABSTRACT

We studied spin Hall effect (SHE) in $Pt_{100-x}Au_x$ with various Au compositions x for Pt-Au/CoFeB systems by means of spin Hall magnetoresistance (SMR). We synthesized low resistive, flat, and highly (111)-textured Pt-Au alloy films by sputtering using low pressure Kr gas. We found that spin Hall angle (θ_{SH}), spin Hall conductivity (σ_{SH}), and spin diffusion length (λ_S) increase by alloying Pt with Au at certain x. The enhancement of σ_{SH} is consistent with the theoretically predicted increase in the intrinsic spin Hall conductivity, however quantitatively, there are some discrepancies in θ_{SH} and λ_S between our result and the experimental and theoretical results in the literatures 19 and 20. The discrepancy between our results and previous results would be related to the difference of the nanostructure in Pt-Au alloys related to the scattering from film surfaces and grain boundaries and the degree of phase separation in Pt-Au alloy systems.

I. INTRODUCTION

Current-induced spin-orbit torque (SOT) originating from the spin-Hall effect (SHE) in heavy metal/ferromagnet (HM/FM) systems has attracted attention due to their potential for application in the efficient manipulation of magnetization in nano-magnets for SOT magnetoresistive random access memory (SOT-MRAM), skyrmion and domain wall devices.[1–16] For their applications, HM with high spin Hall angle $|\theta_{SH}|$ and low resistivity ρ_{xx} is necessary for an efficient SOT operation.[17] An engineering to enhance an intrinsic SHE is one of possible schemes to obtain the HM. A recent *ab initio* electronic structure calculation[18,19] and rigid band model predict that $Pt_{100-x}Au_x$ (x is Au composition) is one of the good candidates for the HM. Actually, a maximum magnitude of $|\theta_{SH}|$ was observed in $Pt_{50}Au_{50}$/NiFe[19] and $Pt_{75}Au_{25}$/Co[20] systems using ferromagnetic resonance (FMR) and harmonic response, and the maximum magnitude of ρ_{xx} was also observed at the same alloy compositions at $x \sim 50$ and $x \sim 25$, respectively. However, it is not clear why alloy compositions x at which the maximum magnitude of $|\theta_{SH}|$ was observed are different between Pt-Au/NiFe[19] and Pt-Au/Co[20] systems. Moreover, there is a discrepancy in the magnitude of the spin diffusion length (λ_S) in Pt-Au between Pt-Au/NiFe[19] and Pt-Au/Co[20] systems. The value of λ_S for $Pt_{75}Au_{25}$/Co system is 1.7 nm, whereas λ_S in Pt-Au/NiFe is an order of magnitude smaller than that in $Pt_{75}Au_{25}$/Co (λ_S ~0.2 nm for $Pt_{50}Au_{50}$/NiFe[19]).

Here, we report results of $|\theta_{SH}|$ and λ_S for $Pt_{100-x}Au_x$ alloys ($0 \leq x \leq 67$) by investigating the spin hall magnetoresistance (SMR) measurements. The SMR measurement is useful method for determining both magnitudes of $|\theta_{SH}|$ and λ_S; therefore, we could accurately evaluate magnitudes of $|\theta_{SH}|$ and λ_S as a function of x. We synthesized flat, highly (111)-textured, and low-resistive Pt-Au alloys by sputtering using low-pressure Kr gas. The maximum magnitude of the

resistivity in the prepared $Pt_{100-x}Au_x$ alloys ($0 \le x \le 67$) is 71.6 $\mu\Omega$cm, which is smaller than the previous reported results.[19,20] We discuss the discrepancy of $|\theta_{SH}|$ and λ_S between the present experiments and the previous theoretical and experimental results[19,20] in terms of the difference in the nanostructure in Pt-Au alloy.

II. EXPERIMENTS

Film stacks, Ta(0.5 nm)/$Co_{20}Fe_{60}B_{20}$(1.5 nm)/Pt(1.5 ~ 7 nm)/Ta(1.0 nm) and Ta(0.5 nm)/$Co_{20}Fe_{60}B_{20}$(1.5 nm)/(Pt(0.4 nm)/Au(y nm))$_n$/Ta(1.0 nm) (y = 0.1, 0.2, 0.4, n: repetition number), and Ta(0.5 nm)/$Co_{20}Fe_{60}B_{20}$(1.5 nm)/(Pt(0.2 nm)/Au(y nm))$_n$/Ta(1.0 nm) (y =0.4) were deposited on thermal oxidized Si substrates by rf magnetron sputtering. Base pressure of the sputtering system was less than 3.5×10^{-7} Pa. We prepared devices with various Pt and Pt-Au alloy film thicknesses varied from ~1.5 to ~7.0 nm. For the preparation of the Pt-Au alloys, we artificial synthesized[17,21] Pt-Au alloys; Pt one monolayer and less than one monolayer Au, or Au one monolayer and less than one monolayer Pt were alternately deposited at room temperature. Kr gas pressure (P_{Kr}) during deposition of the Pt and Pt-Au is P_{Kr} = 0.03 Pa. The easy axis of 1.5 nm thick CoFeB layer lies in in-plane from magnetization measurement using vibrating sample magnetometer (VSM). A dead layer thickness is less than one monolayer (~0.12 nm and ~0.26 nm) for CoFeB/Pt and CoFeB/Pt-Au systems annealed at 300°C, respectively. For all films, the saturation magnetization M_S of $Co_{20}Fe_{60}B_{20}$ is ~1500 emu/cm^3, which is almost the same as that of nominal $Co_{20}Fe_{60}B_{20}$.[22] The result indicates an absence of a significant magnetic proximity effect.[23] After the deposition, the films were patterned into a microscale Hall bar by photolithography and Ar ion milling. Detailed fabrication process was described in the previous paper.[17] The processed wafers were then annealed at 300°C for an hour. We show the typical device photography and the schematic diagram of the devices in Inset of Fig. 2(c). For the measurements of SMR, the current, which is less than equal to 5 μA, is passed through the devices in the *x-axis* direction in Inset of Fig. 2(c) and external magnetic field between -4 and +4 Tesla is applied along either y- and z-axis at 305 K.

III. EXPERIMENTAL RESULTS AND DISCUSSION

Figure 1(a) is the results of x-ray diffraction (XRD) measurements for the stacks with thicknesses of Pt and Pt-Au alloys: t ~7 nm. A standard Cu anode x-ray tube was used to generate x-rays. The results show that Pt and Pt-Au alloys have a face-centered-cubic structure with the (111)-texture. The observed satellite peaks in Fig. 1(a) reminiscent the designed multilayer structure. However, the satellite peaks were also observed in Pt monolayer as shown in Fig. 1(a). In addition, assuming the multilayer formation, the artificial thickness period ($\lambda_{multilayers}$) by using the 2θ distance between XRD main peak and 1st satellite peak is estimated to be $\lambda_{multilayers}$ ~ 3 nm, which is much larger than the designed value of ~ 0.4 ~ 0.8. The possible reason for observing the satellite peaks could originate from flat and high-quality Pt-Au alloy film. It was reported that satellite peaks were also observed in high-quality flat and epitaxial semiconductor film.[24] Therefore, we think the observed satellite peaks and narrow half width at half maximum in XRD patterns indicate the flat and high-quality of the Pt and Pt-Au alloy films prepared. As shown in Fig. 1(a), the peak position of 2θ monotonically decreases with increasing x in $Pt_{100-x}Au_x$ alloys, indicating that lattice constant of Pt-Au increases with increase of Au composition and artificial synthesized (Pt/Au) $_n$ multilayers form Pt-Au alloys. Therefore, from here, we call (Pt (0.4 nm)/Au (y nm))$_n$ (y = 0.1, 0.2, 0.4) and (Pt (0.2 nm)/Au (0.4 nm))$_n$ multilayers $Pt_{100-x}Au_x$ (x = 20, 33, 50, 67 at. %) alloys, respectively. Figures 1(b) and 1(c) show the cross-sectional high-resolution transmission electron microscopy (HR-TEM) images for Ta(0.5 nm)/CoFeB(1.5 nm)/Pt(7 nm)/Ta(1 nm) and Ta(0.5 nm)/CoFeB(1.5 nm)/$Pt_{80}u_{20}$(7 nm)/Ta(1 nm), respectively. Flat and highly (111)-textured Pt and Pt-Au layers were observed. The grain size for both samples is larger than 10 nm.

Figure 2(a) shows the inverse of the device longitudinal resistance ($1/R_{xx}$) multiplied by a geometrical factor (L/w), the sheet conductance, $G_{xx} = L/(wR_{xx})$ values are plotted as a function of the HM layer thickness (t) for all devices, where L = 205 μm and w = 5.1 μm (Inset of Fig. 2(c)). As shown in Fig. 2(a), there is no anomaly for the devices with Pt-Au alloys, indicating no significant change in resistivity with increase of t. On the other hand, there is anomaly at around t ~ 3.5 nm for the devices with Pt; the slope significantly increases at thicker thickness region. The result indicates that the resistivity becomes much smaller at thicker t region. In general, grain size increases with increasing t, leading to decrease of scattering by grain boundary. The solid line in Fig. 2(b) shows the resistivity of Pt calculated using Eq. (23) from the literature 25 which takes into account scattering by both grain boundaries and film surfaces with

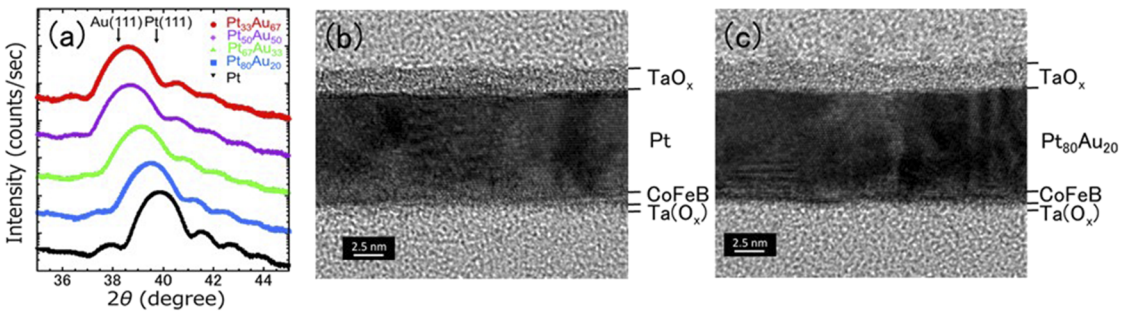

FIG. 1. (a) is result of the out-of-plane x-ray diffraction θ–2θ scan patterns for the stacks with Ta (1 nm)/$Pt_{100-x}Au_x$ (~7 nm)/CoFeB (1.5 nm)/Ta (0.5nm) systems (x = 0, 20, 33, 50, 67). (b) and (c) are results of the cross-section transmission electron microscopy images for Ta(1 nm)/Pt (7 nm)/CoFeB(1.5 nm)/Ta (0.5nm) and Ta(1 nm)/$Pt_{80}Au_{20}$ (~7 nm)/CoFeB(1.5 nm)/Ta (0.5nm) systems on SiO_2/Si substrates.

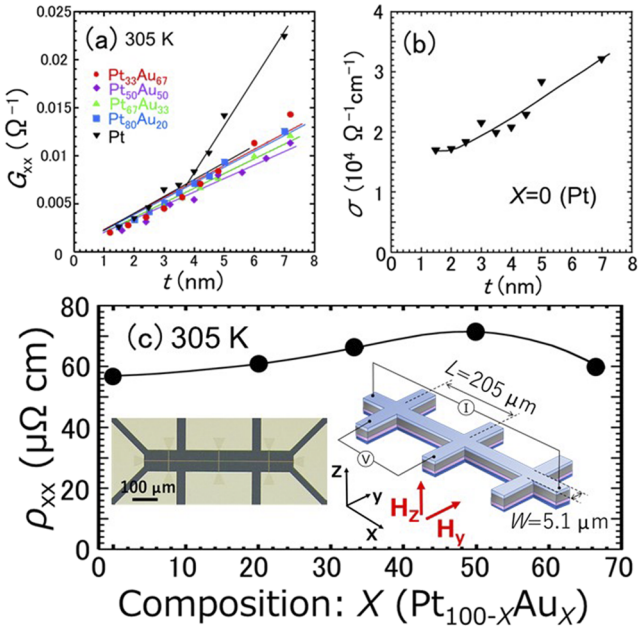

FIG. 2. Sheet conductance (G_{xx}) as a function of Pt-Au thickness (t). The solid lines in (a) are linear fits to the data. (b) is the conductivity (σ) as a function of t for Ta(1 nm)/Pt (t nm)/CoFeB(1.5 nm)/Ta (0.5nm) system. The solid line in (b) is a fit to the data by Eq. (23) from the literature 25. (c) is the resistivity (ρ_{xx}) as a function of Au concentration (x). Insets of (c) are a photograph and schematic diagram of a prepared device.

values $p = 1.0$ fraction of carriers secularly scattered at the surface of Pt layer, bulk resistivity $\rho_\infty = 9$ μΩcm, mean free path $\lambda_{mfp} = 26$ nm and the grain boundary penetration parameter $\zeta = 1.34$, assuming that value of the resistivity (ρ_{CoFeB}) for $Co_{20}Fe_{60}B_{20}$ is $\rho_{CoFeB} = 229$ $\mu\Omega$cm which is the obtained value by the fitting in Fig. 2(a). As shown in Fig. 2(b), the experimental results can be well fitted by the equation, indicating that anomaly in Pt system is related to the scattering from both film surfaces and grain boundaries[24] and scattering due to the grain boundary and surfaces in Pt-Au alloy film is independent on the thickness of the Pt-Au film. The values of ρ_{xx} for the devices with Pt and $Pt_{100-x}Au_x$ alloys are shown in Fig. 2(c). Note that ρ_{xx} in thin thickness region $t \leq 3.5$ nm is plotted for the case of Pt. The estimated ρ_{xx} value has a broad maximum at around $x \sim 50$ at which theoretical work[19] also shows the same tendency. However quantitatively, in terms of the absolute values of ρ_{xx}, there is a discrepancy between our result and the theory 19 assuming the disorder calculated by a coherent potential approximation. The theoretically predicted maximum value of ρ_{xx} for $Pt_{50}Au_{50}$ is about 3 times larger than the ρ_{xx} in Pt. The degree of the increase in ρ_{xx} due to the alloying Pt with Au observed is much smaller than the theoretically predicted increase in ρ_{xx}. This would be related to the good quality (large grains) of our films prepared here.

Figures 3(a) and 3(b) show the typical R_{xx} versus external magnetic field H for the devices with $Pt_{80}Au_{20}$ and the $\Delta R_{XX}/R_{XX}^{H=0}$ as a function of H for the devices with the maximum magnitude of $\Delta R_{XX}/R_{XX}^{H=0}$, respectively. The magnitude of $\Delta R_{XX}/R_{XX}^{H=0}$ saturates at around $|H| = 1.5$–2.0 T, which was consistent with the results of saturation field measured by VSM. As shown in Fig. 3(b), the largest magnitude of $\Delta R_{XX}/R_{XX}^{H=0}$ is observed for the devices with $Pt_{80}Au_{20}$ alloy. Figure 3(c) shows the $\Delta R_{XX}/R_{XX}^{H=0}(H = 2T)$ (average value of $\Delta R_{XX}/R_{XX}^{H=0}$ at H = -2 T and +2 T) as a function of t for all devices. The largest value of $\Delta R_{XX}/R_{XX}^{H=0}(H = 2T)$ is observed for the devices with $Pt_{80}Au_{20}$ alloy. The thickness t at which the maximum values in of $\Delta R_{XX}/R_{XX}^{H=0}(H = 2T)$ vs t plot increases with increasing Au composition x, which indicates the increase in λ_S with increasing x for $Pt_{100-x}Au_x$ alloys. The solid lines in Fig. 3(c) are the results of fit using the following equations[26,27] based on the drift diffusion model[28] to the experimental results.

$$\mathrm{SMR} = \Delta R_{XX}/R_{XX}^{H=0} \sim \theta_{SH}^2 \frac{\lambda_S}{t} \frac{\tanh(t/2\lambda_S)}{1+\xi}\left[1 - \frac{1}{\cosh(t/\lambda_S)}\right], \quad (1)$$

$$\xi \equiv \frac{\rho_{Pt-Au} t_{CoFeB}}{\rho_{CoFeB} t}, \quad (2)$$

where t_{CoFeB} is CoFeB film thickness. The magnitudes of θ_{SH} and λ_S of the Pt-Au HM electrodes are successfully obtained.

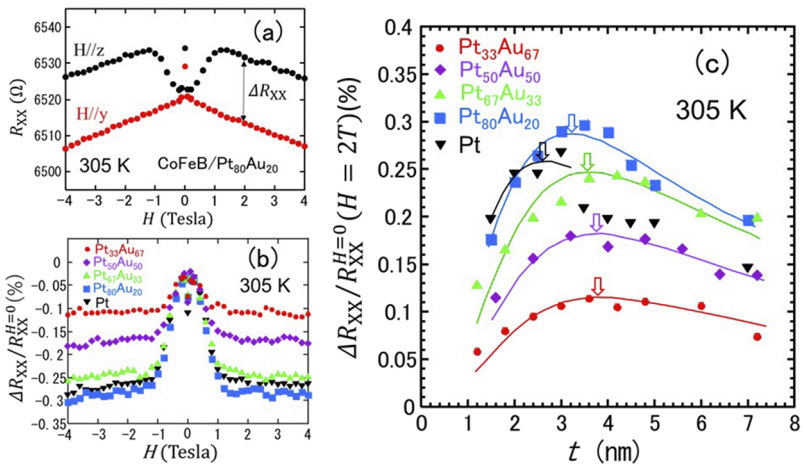

FIG. 3. (a) Typical longitudinal resistance R_{xx} versus external magnetic field H oriented along the y axis (red circles) and z axis (black circles) for the device with 3.5 nm $Pt_{80}Au_{20}$. SMR $\Delta R_{XX}/R_{XX}^{H=0}$ plotted against the (b) H and (c) HM layer thickness t for $Pt_{100-x}Au_x$/CoFeB systems. The solid lines show the fitting results using drift diffusion model.[25,26]

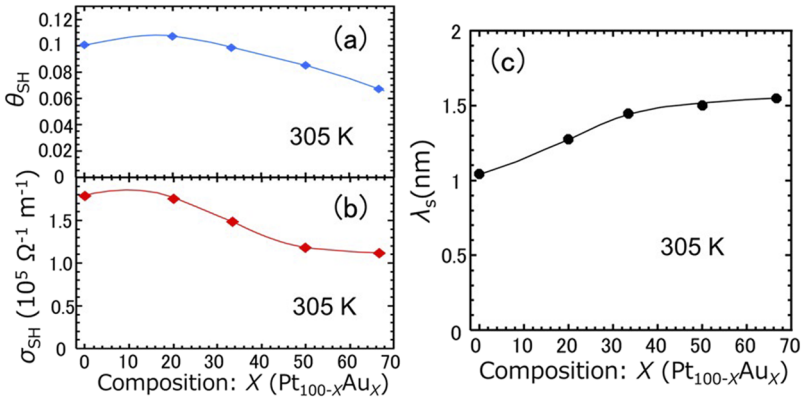

FIG. 4. (a) Estimated magnitude of the Spin Hall angle θ_{SH}, (b) spin hall conductivity σ_{SH} and (c) spin diffusion length λ_S as a function of Au concentration x in the $Pt_{100-x}Au_x$ alloys/CoFeB systems. The solid lines in (a), (b), and (c) are guides for the eyes.

Figures 4(a) and 4(b) show the results of the magnitudes of θ_{SH} and experimentally obtained spin Hall conductivity σ_{SH}, which is more relevant form to compare the results with the calculated intrinsic spin Hall conductivity for bulk Pt[18] and Pt-Au,[19] as a function of x in $Pt_{100-x}Au_x$. The magnitude of θ_{SH} and σ_{SH} has a broad maximum at around x = 20 and between 0 and 20, respectively. The behavior in the determined σ_{SH} shown in Fig. 4(b) is consistent with the reported theoretical and experimental results;[18–20] however, absolute value and the behavior in the experimentally estimated θ_{SH} have large discrepancies between our result and reported results,[19,20] and between the result in Ref. 19 and Ref. 20. The compositions x, and absolute values of θ_{SH} having the maximum values in θ_{SH} are $x = 20$ ($Pt_{80}Au_{20}$), $x = 50$ ($Pt_{50}Au_{50}$) and $x = 25$ ($Pt_{75}Au_{25}$), and +0.11, about +0.3 and +0.35 for our result and experimental results in the literatures 19 and 20, respectively. The theory[19] has suggested that SHE in Pt is dominated by the intrinsic band structure effect and the value of θ_{SH} can be enhanced by alloying Pt with Au by which σ_{SH} is not degraded for raising ρ_{xx}. The degree of the increase in the experimentally determined σ_{SH} for Pt-Au alloys comparing to that for Pt is not so large for all data (our result and literatures 19 and 20). The ratio of the experimentally determined maximum value of ρ_{xx} for Pt-Au alloys to that for Pt: $(\rho_{XX}^{PtAu}/\rho_{XX}^{Pt})$ is $\rho_{XX}^{PtAu}/\rho_{XX}^{Pt}$ = 1.26 for our result. This indicates that the degree of the increase in the θ_{SH} for our result is quantitatively consistent with the theoretically predicted relation of $\theta_{SH} \propto \sigma_{SH}\,\rho_{xx}$. However, the values of ρ_{xx} at $x = 20$ ($Pt_{80}Au_{20}$) for our result, $x = 50$ ($Pt_{50}Au_{50}$) for literature 19 and $x = 25$ ($Pt_{75}Au_{25}$) for literature 20 are 60.9, ~100 and 83 $\mu\Omega$cm, respectively, and the difference of maximum θ_{SH} values between our result and Refs. 19 and 20 could not understand only by the difference in the ρ_{xx} values. The spin scattering would be largely related to not only the increase the ρ_{xx} due to a mixture between Pt and Au but also a nanostructure in Pt-Au layers such as the grain size in Pt-Au. The large grain size of our samples would be one of the reasons for the small values of determined θ_{SH} compared to those of θ_{SH} in the literatures 19 and 20. The equilibrium phase diagram of the Pt-Au system suggests that some phase separation might occur in the prepared film in the composition region between $Pt_{15}Au_{85}$ and Pt. Therefore, the difference in degree of phase separation in Pt-Au alloy systems might be another possible reason for the difference of θ_{SH} values.

Figure 4(c) shows the estimated λ_S as a function of x in $Pt_{100-x}Au_x$. The values of λ_S in Pt-Au alloys are nearly consistent with the previous experimental result in Ref. 20, however, inconsistent with the experimental result in Ref. 19. One order of magnitude smaller λ_S value observed in Pt-Au alloys reported in Ref. 19 compared with our result and Ref. 20 might be also related to the scattering from film surfaces and grain boundaries and the difference in degree of phase separation in Pt-Au alloy systems. More efforts such as correlation between the nanostructure in HM and the value of θ_{SH} and λ_S would be necessary.

IV. CONCLUSIONS

We studied the θ_{SH} and λ_S for $Pt_{100-x}Au_x$/CoFeB system by using SMR measurements and found that both θ_{SH} and λ_S increase by alloying Pt with Au at certain x. The quantitative discrepancy between our results in θ_{SH} and λ_S and previous results would be related to the difference of the nanostructure in Pt-Au alloys related to the scattering from film surfaces and grain boundaries and the degree of phase separation in Pt-Au alloy systems.

ACKNOWLEDGMENTS

This work was partly supported by the JST-OPERA Program (JPMJOP1611) and JSPS KAKENHI (15H05699, 19H00844).

REFERENCES

[1] L. Liu, C.-F. Pai, Y. Li, H. W. Tseng, D. C. Ralph, and R. A. Buhrman, Science **336**, 555 (2012).
[2] G. Yu, P. Upadhyaya, Y. Fan, J. G. Alzate, W. Jiang, K. L. Wong, S. Takei, S. A. Bender, L.-T. Chang, Y. Jiang, M. Lang, J. Tang, Y. Wang, Y. Tserkovnyak, P. K. Amiri, and K. L. Wang, Nat. Nanotechnol. **9**, 548 (2014).
[3] W. Jiang, P. Upadhyaya, W. Zhang, G. Yu, M. B. Jungfleisch, F. Y. Fradin, J. E. Pearson, Y. Tserkovnyak, K. L. Wang, O. Heinonen, S. G. E. Velthuis, and A. Hoffmann, Science **349**, 283 (2015).
[4] P. P. J. Haazen, E. Mure, J. H. Franken, R. Lavrijsen, H. J. M. Swagten, and B. Koopmans, Nat. Mater. **12**, 299 (2013).
[5] A. Chernyshov, M. Overby, X. Liu, J. K. Furdyna, Y. Lyanda-Geller, and L. P. Rokhinson, Nat. Phys. **5**, 656 (2009).
[6] I. M. Miron, K. Garello, G. Gaudin, P.-J. Zermatten, M. V. Costache, S. Auffret, S. Bandiera, B. Rodmacq, A. Schuhl, and P. Gambardella, Nature **476**, 189 (2011).
[7] J. Kim, J. Sinha, M. Hayashi, M. Yamanouchi, S. Fukami, T. Suzuki, S. Mitani, and H. Ohno, Nat. Mater. **12**, 240 (2013).

[8]S. Fukami, T. Anekawa, C. Zhang, and H. Ohno, Nat. Nanotechnol. **11**, 621 (2016).
[9]K.-S. Lee, S.-W. Lee, B.-C. Min, and K.-J. Lee, Appl. Phys. Lett. **104**, 072413 (2014).
[10]K. Garello, C. O. Avci, I. M. Miron, M. Baumgartner, A. Ghosh, S. Auffret, O. Boulle, G. Gaudin, and P. Gambardella, Appl. Phys. Lett. **105**, 212402 (2014).
[11]C. Zhang, S. Fukami, H. Sato, F. Matsukura, and H. Ohno, Appl. Phys. Lett. **107**, 012401 (2015).
[12]M.-H. Nguyen, C.-F. Pai, K. X. Nguyen, D. A. Muller, D. C. Ralph, and R. A. Buhrman, Appl. Phys. Lett. **106**, 222402 (2015).
[13]S. Fukami, T. Anekawa, C. Zhang, and H. Ohno, Nat. Nanotechnol. **10**, 1038 (2016).
[14]S. V. Aradhya, G. E. Rowlands, J. Oh, D. C. Ralph, and R. A. Buhrman, Nano Lett. **16**, 5987 (2016).
[15]M. Baumgartner, K. Garello, J. Mendil, C. O. Avci, E. Grimaldi, C. Murer, J. Feng, M. Gabureac, C. Stamm, Y. Acremann, S. Finizio, S. Wintz, J. Raabe, and P. Gambardella, Nanotechnol. **12**, 980 (2017).
[16]Y. Kato, Y. Saito, H. Yoda, T. Inokuchi, S. Shirotori, N. Shimomura, S. Oikawa, A. Tiwari, M. Ishikawa, M. Shimizu, B. Altansargai, H. Sugiyama, K. Koi, Y. Ohsawa, and A. Kurobe, Phys. Rev. Appl. **10**, 044011 (2018).
[17]Y. Saito, N. Tezuka, S. Ikeda, H. Sato, and T. Endoh, Appl. Phys. Exp. **12**, 053008 (2019).
[18]G. Y. Guo, S. Murakami, T. W. Chen, and N. Nagaosa, Phys. Rev. Lett. **100**, 096401 (2008).
[19]M. Obstbaum, M. Decker, A. K. Greitner, M. Haertinger, T. N. G. Meier, M. Hronseder, K. Chadova, S. Wimmer, D. Ködderitzsch, H. Ebert, and C. H. Back, Phys. Rev. Lett. **117**, 167204 (2016).
[20]L. Zhu, D. C. Ralph, and R. A. Buhrman, Phys. Rev. Appl. **10**, 031001 (2018).
[21]T. Kojima, M. Mizuguchi, T. Koganezawa, K. Osaka, M. Kotsugi, and K. Takanashi, Jpn. J. Appl. Phys. **51**, 010204 (2012).
[22]R. M. Bozorth, *Ferromagnetism* (Wiley-IEEE Press, New York, 1993).
[23]C. L. Canedy, X. W. Li, and G. Xiao, Phys. Rev. B **62**, 508 (2000).
[24]K. W. Shin, S. Song, H.-W. Kim, G.-D. Lee, and E. Yoon, Jpn. J. Appl. Phys. **57**, 065504 (2018).
[25]P. Fan, K. Yi, J.-D. Shao, and A.-X. Fan, J. Appl. Phys. **95**, 2527 (2004).
[26]J. Liu, T. Ohkubo, S. Mitani, K. Hono, and M. Hayashi, Appl. Phys. Lett. **107**, 232408 (2015).
[27]J. Kim, P. Sheng, S. Takahashi, S. Mitani, and M. Hayashi, Phys. Rev. Lett. **116**, 097201 (2016).
[28]V. P. Amin and M. D. Stiles, Phys. Rev. B **94**, 104420 (2016).